Human Molecular Genetics, 2010, Vol. 19, No. 22 ***4373–4384***
doi:10.1093/hmg/ddq358
Advance Access published on August 25, 2010

The Huntington's disease mutation impairs Huntingtin's role in the transport of NF-κB from the synapse to the nucleus

Edoardo Marcora and Mary B. Kennedy*

Division of Biology, California Institute of Technology, 1200 E California Blvd, M/C 216-76, Pasadena, CA 91125, USA

Received June 8, 2010; Revised August 5, 2010; Accepted August 18, 2010

Expansion of a polyglutamine (polyQ) tract in the Huntingtin (Htt) protein causes Huntington's disease (HD), a fatal inherited neurodegenerative disorder. Loss of the normal function of Htt is thought to be an important pathogenetic component of HD. However, the function of wild-type Htt is not well defined. Htt is thought to be a multifunctional protein that plays distinct roles in several biological processes, including synaptic transmission, intracellular transport and neuronal transcription. Here, we show with biochemical and live cell imaging studies that wild-type Htt stimulates the transport of nuclear factor κ light-chain-enhancer of activated B cells (NF-κB) out of dendritic spines (where NF-κB is activated by excitatory synaptic input) and supports a high level of active NF-κB in neuronal nuclei (where NF-κB stimulates the transcription of target genes). We show that this novel function of Htt is impaired by the polyQ expansion and thus may contribute to the etiology of HD.

INTRODUCTION

Huntington's disease (HD) is an autosomal dominant neurodegenerative disorder caused by expansion of a CAG trinucleotide repeat in the *huntingtin* (*HTT*) gene, which translates into an abnormally long polyglutamine (polyQ) tract in the Huntingtin (Htt) protein (1). HD is characterized by late onset motor, cognitive and psychiatric disturbances that progress to death. Clinical symptoms are accompanied by neuronal dysfunction and loss, particularly in the cerebral cortex and corpus striatum (2).

It is well established that wild-type Htt is neuroprotective (3–6) and that loss of the normal function of Htt can contribute to the HD phenotype (7–9). Nonetheless, the normal function of Htt remains poorly defined.

Htt has been separately implicated in at least three distinct cellular processes (10): neuronal transcription, intracellular transport and synaptic transmission. Of these three, the role of Htt as a modulator of neuronal transcription is particularly well documented. For example, wild-type Htt interacts with transcription factors such as neurogenic differentiation [NeuroD (11)] and RE1-silencing transcription factor/neuron-restrictive silencer factor [REST/NRSF (12,13)] to promote the establishment and maintenance of neuron-specific transcriptional programs, which are critical for neuronal development and survival. Wild-type Htt also interacts with nuclear factor κ light-chain-enhancer of activated B cells [NF-κB (14)] that has been recently implicated in neural-specific functions (15), including synaptic plasticity, neuroprotection and activity-dependent brain-derived neurotrophic factor (BDNF) expression (16–19). In non-neuronal cells, NF-κB is normally kept in an inactive state outside the nucleus; however, in neurons, basal glutamatergic transmission constitutively activates NF-κB (20,21). Of all the transcription factors that respond to excitatory synaptic input, NF-κB is the only one yet shown to be activated locally inside synapses (21,22). Following its activation, NF-κB is retrogradely transported along dendrites to the soma where it is imported into the nucleus (21,23). It had not been previously known whether there is a relationship between binding of Htt to NF-κB and activation of NF-κB at synapses or transport of NF-κB from the synapse to the nucleus.

A second process in which Htt has been suggested to play a role is intracellular transport. Specifically, Htt has been shown to interact with cytosplasmic dynein, a motor protein that drives cargoes along microtubular tracks toward the minus end (24). Wild-type Htt binds to dynein in a complex with dynactin and Htt-associated protein-1 (HAP1) to facilitate

*To whom correspondence should be addressed. Tel: +1 6263953923; Fax: +1 6263958474; Email: kennedym@caltech.edu

the transport of vesicles and mitochondria (24–27). The polyQ expansion interferes with this function of Htt and causes slower intracellular transport of vesicles and mitochondria (25–27). Retrograde transport of NF-κB along dendrites toward the nucleus is mediated by cytoplasmic dynein (28), but a role for Htt in this process had not been previously investigated.

Finally, the notion that Htt may be involved in synaptic transmission arose from the fact that the proline-rich domain of Htt binds to the SH3 domain of PSD-95 (29). PSD-95 is a neuronal scaffold protein (30) that links synaptic glutamate receptors, cell adhesion molecules, signal transducing enzymes and cytoskeletal elements in the PSD, an intricate protein complex located beneath the plasma membrane of dendritic spines at the point of contact with the axon terminal (31). The biological significance of the binding of Htt to PSD-95 remains unclear (32).

Here, we report a new functional role of Htt in the transport of NF-κB from the synapse to the nucleus that involves all three of these proposed cellular functions of Htt in an integrated biological process. We show that transport of NF-κB out of dendritic spines and its activity in neuronal nuclei is reduced by the HD mutation and thus may contribute to the etiology of HD.

RESULTS

Htt and NF-κB are present in the PSD fraction

PSD-95 and Htt have been shown to interact in brain lysates (29), and PSD-95 is highly enriched in both the PSD fraction and in the intact PSD *in vivo* (30,33,34). In contrast, Htt has a broad subcellular distribution (35). Therefore, we asked whether the interaction with PSD-95 causes a portion of Htt to localize to the PSD fraction. We measured the content of Htt in subcellular fractions obtained from adult rat forebrains (Fig. 1A and B). The results confirm that Htt has a broad subcellular distribution and is found in the cytosolic (S3), microsomal (P3), synaptosomal (SS) and clathrin-coated vesicle (CCV) fractions. HAP1, a protein that has previously been found to bind to Htt, has the same distribution (36,37). However, in addition to their localization in these fractions, we found that both Htt and HAP1 are present in the PSD fraction.

We applied two additional tests to confirm that Htt interacts directly with PSD-95 in the PSD fraction. The PSD fraction can be separated into a high-density component devoid of lipid and a low-density component that corresponds to neuronal lipid rafts (38,39). We found that Htt and HAP1 are located only in the high-density component where they co-migrate with a portion of PSD-95 (Fig. 1C). We were also able to coimmunoprecipitate Htt and PSD-95 from a PSD fraction that had been partially solubilized in alkaline deoxycholate as described in Blahos and Wenthold (40), Figure 2A. In contrast, synGAP, a protein that is highly enriched in the PSD (41) and associates with PSD-95 but not Htt, does not coimmunoprecipitate with Htt. These results support the hypothesis that the PSD is the subcellular locale where Htt and PSD-95 interact.

We estimated the equilibrium dissociation constant (K_d) for the interaction between Htt and PSD-95 by measuring the affinity of a recombinant exon 1 fragment of wild-type Htt for full-length recombinant PSD-95 in a modified enzyme-linked sorbent assay (ELSA; Fig. 2B). The measured K_d of 0.8 ± 0.12 μM indicates that Htt and PSD-95 interact with a biologically meaningful affinity in the same range (0.1–8 μM) as other SH3/proline-rich domain-mediated interactions (42).

Because wild-type Htt has been reported to bind to the p50 subunit of NF-κB (14), we investigated whether NF-κB is also found in the PSD fraction. Active NF-κB has been recovered from synaptosomal preparations after stimulation with glutamate (21,22). However, synaptosomes contain both pre- and postsynaptic compartments and it has not been established whether synaptic activation of NF-κB is a pre- or a postsynaptic event. Although NF-κB and inhibitor of κB (I-κB) have been visualized in the PSD by electron microscopic immunocytochemistry (43), their presence in the PSD fraction had not been established. We used a mini-prep method that we developed for rapid and convenient purification of the PSD fraction from a single mouse forebrain (Fig. 3A) to examine this issue. We found that both the p50 and p65 subunits of NF-κB are indeed present in the PSD fraction (Fig. 3B). Moreover, we found that the phosphorylated form of I-κBα is highly enriched in the PSD fraction compared with homogenate and synaptosomes. Phosphorylation of I-κBα initiates the process of NF-κB activation. Interestingly, we also found that I-κB is a substrate for Ca^{2+}/calmodulin-dependent protein kinase II (CaMKII), a major protein kinase in the PSD (Supplementary Material, Fig. S1). Thus, the PSD may be a site at which NF-κB is preferentially activated in the synapse.

The HD mutation impairs localization of Htt in the PSD fraction

Sun *et al*. (29) reported that the HD mutation interferes with binding of Htt to PSD-95. If binding to PSD-95 is important for localization of Htt to the PSD, then the HD mutation should reduce the association of Htt with the PSD fraction. To test whether this is true, we used the PSD mini-prep method to compare the molecular composition of the PSD fraction between individual mouse mutants. We measured the amounts of Htt, the Htt-associated protein HAP1 and several other proteins known to be enriched in the PSD fraction at various ages in wild-type and HD knock-in mice in which an expanded stretch of 140 CAG repeats is inserted into the first exon of the mouse *Htt* gene by homologous recombination (44,45). The HD mutation reduced the amount of Htt in the PSD fraction to 45 ± 6 and $35 \pm 4\%$ of that in young adult and aged wild-type control mice (6 months and 2 years of age, respectively, $n = 4$) (Fig. 4A and B). The Htt-associated protein HAP1 showed an opposite trend toward increased levels in the PSD fraction from HD knock-in mice, although the trend was not statistically significant. The latter result suggests that HAP1 may anchor itself to the PSD independently of its interaction with Htt, perhaps via its interaction with other PSD proteins such as Kalirin-7 (46,47). The levels of synGAP, CaMKII and PSD-95 were not significantly altered in the PSD fraction from HD knock-in mice.

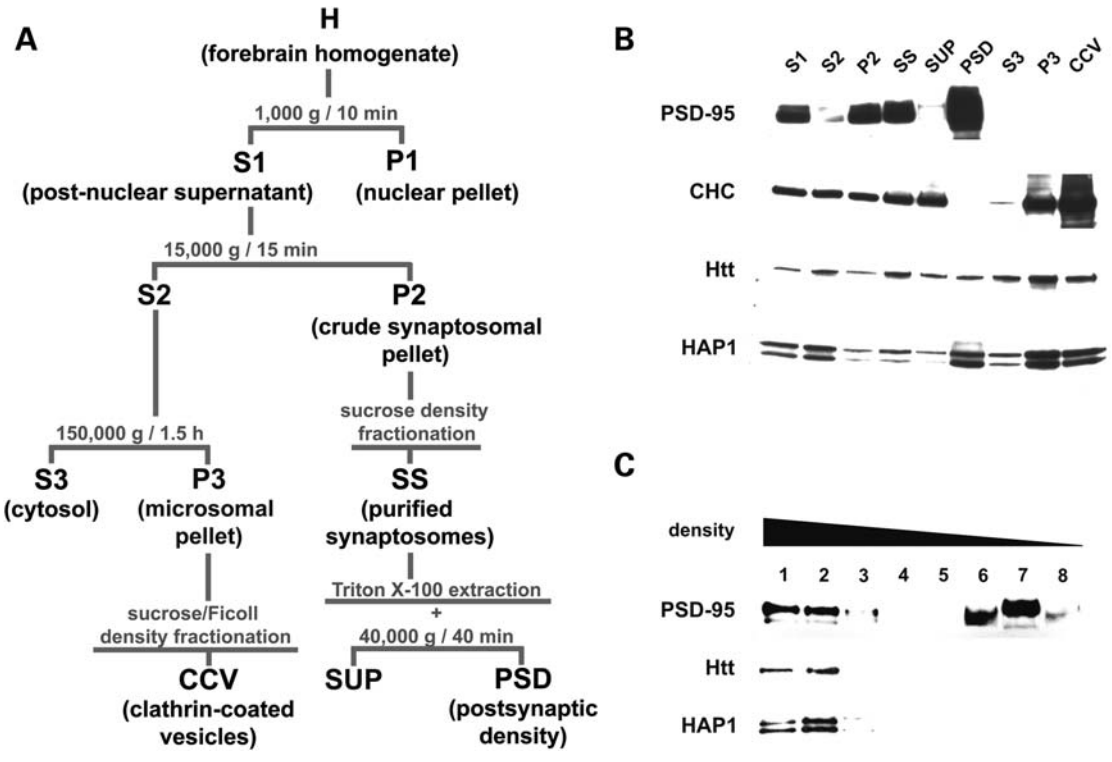

Figure 1. Htt is present in the PSD fraction. (**A**) Schematic diagram of the procedures used for subcellular fractionation of adult rat forebrains. (**B**) Representative immunoblot ($n = 4$) of subcellular fractions (40 μg of total protein) prepared from adult rat forebrains by differential and density-gradient centrifugation. PSD-95 (a postsynaptic density marker), clathrin heavy chain (CHC, a clathrin-coated vesicle marker), Huntingtin (Htt) and Huntingtin-associated protein 1 (HAP1) were detected as described in Materials and Methods. (**C**) Representative immunoblot ($n = 2$) of sequential fractions (40 μl), collected beginning from the bottom of the tube, after ultracentrifugation of a PSD fraction through an OptiPrep (Axis-Shield) density gradient (lanes 1–8, from high to low density). PSD-95, Htt and HAP1 were detected as described in Materials and Methods. H, forebrain homogenate; S1, post-nuclear supernatant; P1, nuclear pellet; S2, medium speed supernatant of S1; P2, crude synaptosomal pellet; SS, purified synaptosomal fraction derived from P2; SUP, high-speed supernatant of SS extracted with Triton X-100; PSD, postsynaptic density fraction; S3, cytosol; P3, microsomal pellet; CCV, clathrin-coated vesicles derived from P3.

Taken together, our data demonstrate that a portion of neuronal Htt localizes to the PSD fraction where it interacts with PSD-95. The HD mutation impairs localization of Htt in the PSD fraction, suggesting that any functional role of Htt in the PSD may also be impaired by the HD mutation.

Htt interacts preferentially with active NF-κB

The localization of both Htt and NF-κB in the PSD fraction led us to investigate whether Htt might play a role in the activation of NF-κB inside synapses upon stimulation of glutamate receptors (21). In the absence of stimuli, NF-κB is kept in an inactive state outside the nucleus by binding to an inhibitory protein of the I-κB family, which masks the nuclear localization signal (NLS) and the DNA-binding domain of NF-κB. Phosphorylation of I-κB at specific serine residues (for instance, serines 32 and 36 of I-κBα) directs I-κB to the ubiquitin-proteasome system (UBS) to be degraded and activates NF-κB by releasing it for nuclear import and DNA binding (48).

We considered two hypothetical models for a role of Htt in the postsynaptic activation of NF-κB. Htt might interact with inactive NF-κB and anchor it to the PSD by binding to PSD-95, facilitating the activation of NF-κB by the signal transduction machinery associated with glutamate receptors. Alternatively, Htt might interact preferentially with active NF-κB and facilitate its transport from the PSD to the nucleus by binding to the dynein–dynactin motor complex. As a first step to distinguish between these two hypotheses, we asked whether Htt interacts with active or inactive NF-κB.

Htt has previously been shown to bind to the p50 subunit of NF-κB in HeLa cells (14). The synaptic form of NF-κB is a heterodimer composed of p50 and p65 subunits; therefore, we first tested whether Htt can also interact with the p65 subunit. We found that Htt coimmunoprecipitates with p65 from HeLa cell lysates (Fig. 5A, lane 1). To test whether this interaction is changed by activation of NF-κB, we treated the HeLa cells with tumor necrosis factor-α (TNF-α) to activate NF-κB prior to immunoprecipitation. The treatment increased the amount of p65 immunoprecipitating with Htt by 193 ± 35% relative to the untreated controls ($n = 3$) (Fig. 5A, compare lane 1 with lane 4). Quantitation was performed by fluorescent immunoblot as described in Materials and Methods. These data suggest that Htt binds preferentially to the activated form of NF-κB.

As part of the process of activation of NF-κB, I-κB is degraded, exposing the NLS of NF-κB which then binds to a member of the importin-α family (49). Members of the importin-α family bind to a variety of NLS-containing proteins and form a complex with importin-β1. The importin complex mediates the translocation of these proteins from the cytoplasm into the nucleus through the nuclear pore complex (50). Therefore, to further probe the state of

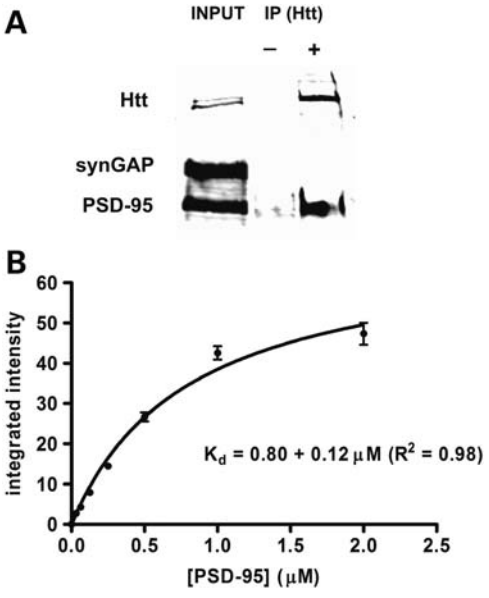

Figure 2. Htt interacts with PSD-95 in the PSD fraction. (**A**) Representative immunoblot of proteins immunoprecipitated (IP) from a solubilized PSD fraction prepared from adult rat forebrains (INPUT, 5% of total input; 20 μg of total protein) by incubation with protein G magnetic beads pre-coated with an antibody against Htt (+) or with an isotype control antibody (−). Huntingtin (Htt), synGAP and PSD-95 were detected as described in Materials and Methods. The experiment was performed twice under the conditions shown and twice under slightly different detergent conditions with the same result ($n = 4$). (**B**) Binding of full-length PSD-95 to the N-terminal portion of Htt corresponding to exon 1, immobilized in a microplate well. Data ($n = 3$) were obtained by a modified enzyme-linked sorbent assay (ELSA) in which the integrated intensity of the fluorescence emitted by a fluorophore-labeled antibody against PSD-95 is measured with a fluorescence microplate reader.

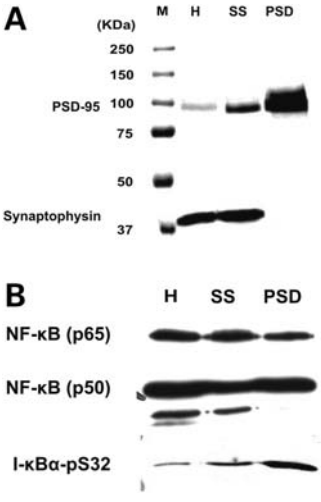

Figure 3. NF-κB is present in the PSD fraction. (**A**) Representative immunoblot ($n = 4$) of subcellular fractions (20 μg of total protein) prepared from a single adult mouse forebrain by differential and density gradient centrifugation. PSD-95 (a postsynaptic marker) and Synaptophysin (a presynaptic marker) were detected as described in Materials and Methods. M, molecular weight marker; H, forebrain homogenate; SS, purified synaptosomal fraction derived from H; PSD, postsynaptic density fraction derived from SS extracted with Triton X-100. (**B**) Representative immunoblot ($n = 4$) of subcellular fractions (40 μg of total protein) prepared from a single adult mouse forebrain by differential and density gradient centrifugation. The p65 and p50 subunits of NF-κB, and I-κBα phosphorylated on serine 32 (I-κBα-pS32) were detected as described in Materials and Methods. H, forebrain homogenate; SS, purified synaptosomal fraction derived from H; PSD, postsynaptic density fraction derived from SS extracted with Triton X-100.

activation of NF-κB in Htt immunoprecipitates, we tested for the presence of I-κBα, which would be in the complex only if NF-κB is inactive, and for importin-α, which would be present only if NF-κB is active.

We decided to test specifically for importin-α2, because its localization and behavior in neurons is very similar to that of NF-κB. For example, it has been shown to localize to the PSD (51 and Fig. 5B) and to translocate from the synapse to the nucleus upon stimulation of glutamate receptors (51). We found that importin-α2 coimmunoprecipitates with NF-κB (Fig. 5C) and with Htt and p65 from HeLa cell lysates (Fig. 5A), whereas I-κBα does not. Furthermore, importin-α2 was detectable in the immunoprecipitates only when NF-κB was activated by treatment with TNF-α (Fig. 5A, compare lanes 2 and 5). The level of importin-α2 in lane 2 was not statistically significantly different from the control level in lane 3, whereas the level in lane 5 was significantly greater than the control level in lane 6 ($P = 0.02$, $n = 3$). These results strengthen the conclusion that Htt preferentially interacts with the activated form of NF-κB.

Both loss of Htt function and the HD mutation slow the rate of movement of NF-κB out of activated dendritic spines

A general role of wild-type Htt in stimulating intracellular transport events mediated by the dynein–dynactin motor complex is well established. For example, downregulation of Htt expression by RNAi or deletion of Htt by conditional gene targeting causes substantially slower intracellular transport of vesicles and mitochondria (24–26). Htt appears to stimulate retrograde transport of various cargoes through its binding to dynein intermediate chain (24) and to HAP1 (25), which interacts directly with the $p150^{Glued}$ subunit of dynactin (52,53).

Our finding that Htt interacts preferentially with the activated form of NF-κB (Fig. 5A) and the fact that the dynein–dynactin motor complex is required for the retrograde transport of NF-κB in dendrites upon stimulation of glutamate receptors (28), prompted us to investigate whether Htt plays a role in the transport of NF-κB from dendritic spines to the nucleus. To visualize movement of NF-κB out of dendritic spines, we transfected mature neurons cultured for 14 days *in vitro* with the p65 subunit of NF-κB tagged with a photoactivatable variant of GFP [paGFP–p65 (54)] and used two-photon laser excitation to photoactivate paGFP–p65 within a single spine (55), Figure 6A. To determine the rate of activity-dependent NF-κB movement out of dendritic spines, we first bathed the neurons in tetrodotoxin (TTX) for 12 h and then removed the TTX to initiate action potentials. After TTX washout, we photoactivated the paGFP–p65 in single spines. We then made repeated time-lapse measurements of fluorescence intensity within each targeted spine and fitted the decay curve with a single exponential to obtain the half-life of fluorescence decay. To correct for the decay of fluorescence caused by photobleaching, we repeated the measurements in the same neurons after chemical fixation.

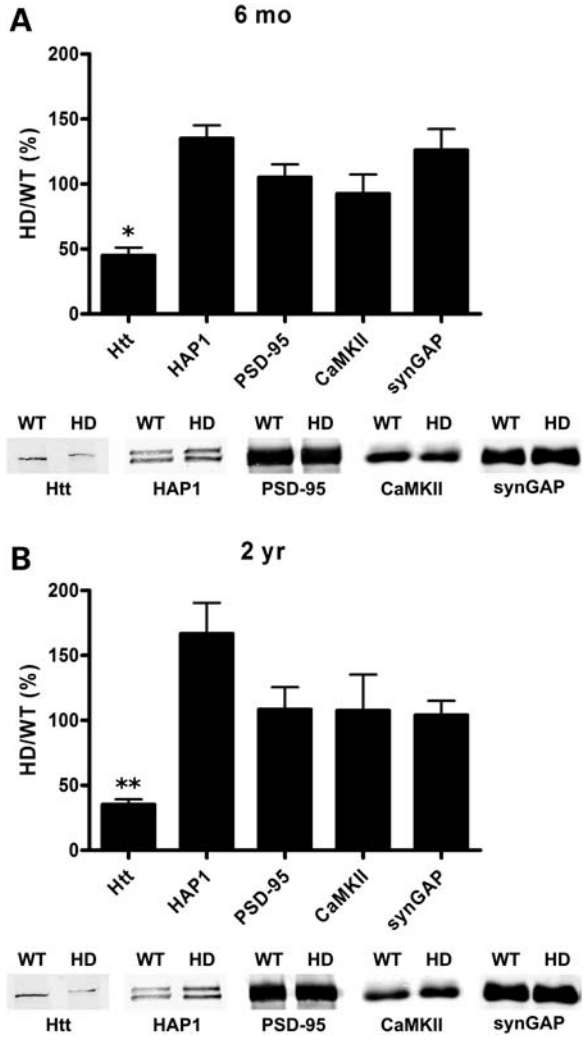

Figure 4. The HD mutation impairs localization of Htt in the PSD fraction. (**A**) Mean amount of indicated proteins in PSD fractions (40 μg of total protein) prepared from forebrains of 6-month-old (6 mo) HD knock-in (HD) mice, plotted as percentage relative to wild-type control (WT) mice ($n = 4$ non-sex matched, littermate pairs). Protein quantitation was performed by immunoblotting as described in Materials and Methods. Representative blots are shown below the graph. Error bars represent SEM. $^{*}P < 0.05$, $^{**}P < 0.01$; two-tailed paired *t*-test. (**B**) Same as (A) but using 2-year-old (2 yr) mice ($n = 4$ non-sex matched, littermate pairs).

We first compared the activity-dependent movement of NF-κB out of spines in live cortical pyramidal neurons cultured from mice with a conditional knock-out of *Htt* targeted to pyramidal neurons (4) and in neurons from control mice lacking the *Cre* transgene. After correction for photobleaching, the half-life for movement of NF-κB out of dendritic spines in control neurons was 21 ± 5 s (Fig. 6B and C). In neurons from which *Htt* was deleted, the half-life was 58 ± 11 s, more than double that of controls (Fig. 6B and C). These results demonstrate that wild-type Htt stimulates the rate of activity-dependent movement of NF-κB out of dendritic spines.

The HD mutation is known to impair the ability of Htt to stimulate intracellular transport of organelle cargoes carried by the dynein–dynactin motor complex (25,26). Therefore, we next determined whether the HD mutation also interferes with the activity-dependent movement of NF-κB out of dendritic spines. We compared the transport of NF-κB in wild-type neurons and neurons isolated from HD knock-in mice. After correction for photobleaching, the half-life for movement of NF-κB out of dendritic spines in HD neurons was 75 ± 7 s compared to 36 ± 3 s in wild-type neurons (Fig. 6D and E). These results indicate that the HD mutation is sufficient to slow the rate of NF-κB movement out of dendritic spines.

To confirm that this movement is driven by synaptic activity, we measured the transport of NF-κB in wild-type neurons before and after TTX washout and found, as expected, that the half-life of fluorescence decay was 230 ± 24 s before TTX washout and 37 ± 1 s after ($n = 2$, data not shown).

Both loss of Htt function and the HD mutation reduce the concentration of active NF-κB in neuronal nuclei

Because excitatory synaptic input is the major physiological inducer of NF-κB activity in neurons (20,21), we hypothesized that loss of Htt function should reduce the movement of active NF-κB along the dendrite toward the soma, ultimately reducing the amount of active NF-κB in the nucleus. We were not able to track the movement of NF-κB after it left the dendritic spine, because fluorescent NF-κB rapidly disperses in the dendrite and does not concentrate in large transport particles or vesicles. Therefore, we investigated whether the transport defects that we observe at the synapse correlate with decreased levels of active NF-κB in the nucleus. We prepared extracts of a neuronal nuclear fraction from forebrains of 4-month-old Htt knock-out mice, 6-month-old HD knock-in mice and the corresponding controls. The amount of active NF-κB in the extracts was measured by a DNA pull-down assay. We used double-stranded DNA oligonucleotides containing a known consensus binding site for the activated form of NF-κB, termed a κB site. Oligonucleotides containing a mutated κB site that does not bind NF-κB were used as negative control. Htt knock-out mice had reduced levels of active NF-κB ($24 \pm 8\%$ of controls, $n = 2$) in the nuclei of forebrain neurons (Fig. 7A). An even more severe reduction was observed in HD knock-in mice ($11 \pm 3\%$ of controls, $n = 2$; Fig. 7B). The total NF-κB was also reduced in the nuclear fraction, albeit not as substantially as active NF-κB ($75 \pm 2\%$ of controls in Htt knock-out mice and $63 \pm 1\%$ of controls in HD knock-in mice, $n = 2$; Fig. 7A and B, respectively). These data are consistent with the prediction that in neurons from Htt knock-out and HD knock-in mice, impaired transport of NF-κB from distal synaptic sites will result in a reduced level of active NF-κB in the nucleus.

DISCUSSION

The major finding reported here is that Htt stimulates the rate of activity-dependent transport of NF-κB out of dendritic spines, where NF-κB is tonically activated by ongoing synaptic activity (20,21). Furthermore, we have shown that the HD mutation interferes with this novel function of Htt, suggesting that impaired transport of NF-κB from the synapse to the

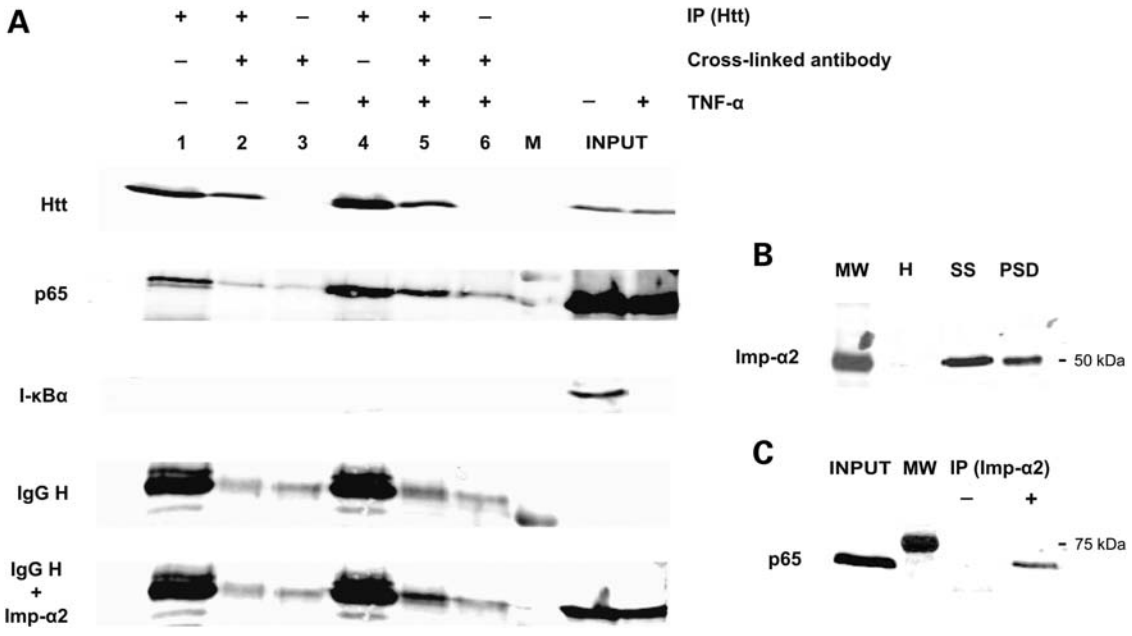

Figure 5. Htt interacts preferentially with active NF-κB. (**A**) Representative immunoblot of proteins immunoprecipitated (IP) from HeLa cell lysates (INPUT, 10% of total input; 40 μg of total protein) by incubation with protein G magnetic beads pre-coated with antibody against Htt (+, lanes 1–2 and 4–5) or with an isotype control antibody (−, lanes 3 and 6). The p65 subunit of NF-κB, total I-κBα, Importin-α2 (Imp-α2) and mouse IgG (IgG H) were detected as described in Materials and Methods. Lanes 2–3 and 5–6 contain precipitates from beads covalently bound to Htt and control antibodies by a cross-linking reagent to enable elution of the immunoprecipitated proteins without contamination by heavy and light chains of IgG. Lanes 1–3 (−TNF-α) contain precipitates from lysates of cells that were not treated TNF-α. Lanes 4–6 (+TNF-α) contain precipitates from lysates of cells that had been treated with TNF-α to activate NF-κB, as described in Materials and Methods. The experiment was performed twice under the conditions shown and once under slightly different detergent conditions with the same result ($n = 3$). (**B**) Immunoblot of subcellular fractions (40 μg of total protein) prepared from a single adult mouse forebrain by differential and density gradient centrifugation. Importin-α2 (Imp-α2) was detected in the PSD as described in Materials and Methods and as previously shown by Thompson *et al*. (51). H, forebrain homogenate; SS, purified synaptosomal fraction derived from H; PSD, postsynaptic density fraction derived from SS extracted with Triton X-100; MW, molecular weight marker. (**C**) Representative immunoblot of proteins immunoprecipitated (IP) from lysates of HeLa cells that had been treated with TNF-α as described in (B; INPUT, 10% of total input; 40 μg of total protein) by incubation with protein G magnetic beads pre-coated with antibody against Imp-α2 (+) or isotype control antibody (−). The p65 subunit of NF-κB was detected as described in Materials and Methods. The immunoblot was performed twice under the conditions shown and once under slightly different detergent conditions with the same result ($n = 3$). MW, molecular weight markers.

nucleus may contribute to the etiology of HD. Consistent with this proposed function of Htt, we have shown that it is present in the PSD fraction where it interacts with PSD-95, a major PSD scaffold protein. The polyQ expansion interferes with the localization of Htt to the PSD fraction, presumably because of its decreased affinity for PSD-95 (29). We also confirmed that NF-κB and I-κB are located in the PSD. Our finding that I-κB is a substrate for Ca^{2+}/calmodulin-dependent protein kinase II (CaMKII), a major protein kinase in the PSD (Supplementary Material, Fig. S1), suggests a potential molecular mechanism by which stimulation of synaptic glutamate receptors might rapidly and locally activate NF-κB in the PSD. We also found that Htt associates preferentially with the activated form of NF-κB and importin-α2, which is involved in the translocation of active NF-κB across the nuclear pore into the nucleus (49). Wild-type Htt is believed to be a multifunctional protein and it has been implicated in several distinct cellular processes, including synaptic transmission, intracellular transport and neuronal transcription. Our findings show that all three of these apparently independent processes are facets of the role that Htt plays in the activity-dependent transport of the transcription factor NF-κB out of dendritic spines.

A steady flow of active NF-κB from distal synaptic sites to the nucleus is needed to sustain the high basal levels of nuclear NF-κB activity observed in neurons (21,28). Loss of Htt function, resulting from a null mutation or the polyQ expansion, could limit the amount of active NF-κB in the nucleus, as we have observed in forebrain neurons from Htt knock-out and HD knock-in mice. This low basal level of nuclear NF-κB activity in neurons could result in weakened neuroprotective transcriptional responses associated with NF-κB and therefore contribute to the etiology of HD.

A myriad of molecular and cellular dysfunctions have been observed in models of HD. Therefore, it is possible that the low constitutive nuclear NF-κB activity that we observed in forebrain neurons of HD mice is caused by a different impairment unrelated to Htt-mediated transport of NF-κB from the synapse to the nucleus. For example, the HD mutation could lead to defective activation of NF-κB in synapses by altering synaptic transmission (56,57) or by inhibiting UBS-mediated proteolysis of I-κB in the PSD (58). In general, however, these dysfunctions are much milder and more slowly progressing in full-length Htt knock-in mouse models of HD than in models generated by overexpression of very long polyQ tracts in the context of very short N-terminal fragments of Htt. For example, baseline synaptic transmission was found to be normal in HD knock-in mice up to 4 months of age (59). In addition, reduced UBS-mediated proteolysis has been observed in HD knock-in mice only after 1 year of age (58).

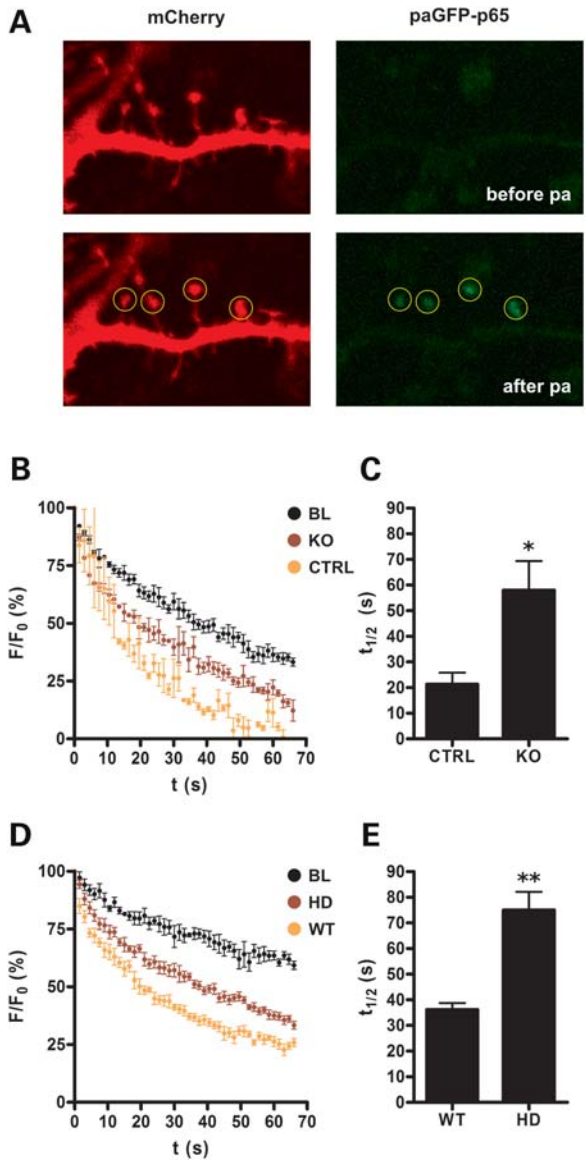

Figure 6. Both loss of Htt function and the HD mutation slow the rate of movement of NF-κB out of activated dendritic spines. (**A**) Dendritic segment of a cultured cortical pyramidal neuron (15 days *in vitro*) that was transiently transfected with mCherry (red channel, left) and with photoactivatable green fluorescent protein fused to the p65 subunit of NF-κB (paGFP–p65; green channel, right), as described in Materials and Methods. Circles indicate dendritic spines in which paGFP–p65 was photoactivated by targeted two-photon laser radiation. The green channel on the right shows the fluorescence of paGFP–p65 before (top) and after (bottom) photoactivation. (**B**) Time course of paGFP–p65 fluorescence after photoactivation in single dendritic spines of live cortical pyramidal neurons derived from Htt knock-out (red dots, KO) and control (yellow dots, CTRL) mice, in a representative time-lapse experiment. Decay of paGFP–p65 fluorescence due to photobleaching (black dots, BL) was measured as the time course of paGFP–p65 fluorescence after photoactivation in single dendritic spines of the same neurons after chemical fixation. paGFP–p65 fluorescence is plotted over time (t) as percent of fluorescence at the time of photoactivation (F/F_0). (**C**) Mean half-life ($t_{\frac{1}{2}}$) of paGFP–p65 fluorescence decay (fitted with a single exponential and corrected for photobleaching) after photoactivation in single dendritic spines ($n = 3$ non-sex matched, littermate pairs [21/59 neurons/spines]). (**D** and **E**) Same as (B) and (C), except that neurons were prepared from HD knock-in (HD) and wild-type control (WT) mice ($n = 5$ non-sex matched, littermate pairs [32/93 neurons/spines]). Error bars represent SEM. $^{*}P < 0.05$, $^{**}P < 0.01$; two-tailed paired t-test.

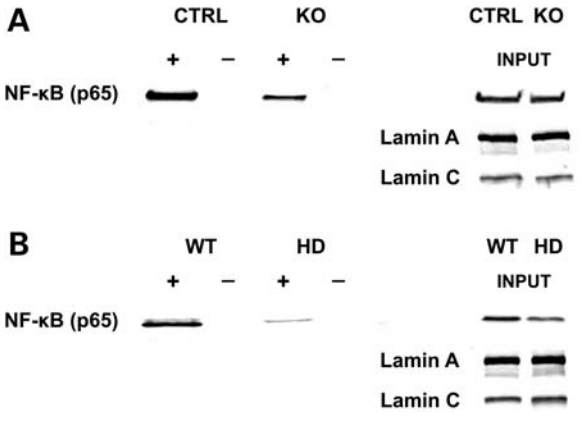

Figure 7. Both loss of Htt function and the HD mutation reduce the concentration of active NF-κB in neuronal nuclei. Representative immunoblots of active NF-κB purified from neuronal nuclear extracts (100 μg of total protein) by incubation with streptavidin magnetic beads pre-coated with biotinylated double-stranded DNA oligonucleotides containing the κB site (+) or a negative control sequence (−). The p65 subunit of NF-κB and Lamin A/C (nuclear markers) were detected as described in Materials and Methods. Extracts (INPUT, 10% of total input; 10 μg of total protein) were obtained from neuronal nuclear fractions prepared from forebrains of (**A**) 4-month-old Htt knock-out (KO) and control (CTRL) mice ($n = 2$ non-sex matched, littermate pairs) and (**B**) 6-month-old HD knock-in (HD) and wild-type control (WT) mice ($n = 2$ non-sex matched, littermate pairs). See text for quantification of the immunoblots.

Our proposed role of Htt in the transport of NF-κB from the synapse to the nucleus is also supported by the fact that we see the correlation of defective transport of NF-κB and reduced level of NF-κB in neuronal nuclei in both HD knock-in and Htt knock-out mice. Of all dysfunctions reported in HD mutant mice, only defective transport of membranous organelles (26) and abnormal nuclear activity of the transcription factor REST/NRSF (13) have also been reported in Htt knock-out mice. Interestingly, abnormal levels of REST/NRSF activity in the nucleus could also be the consequence of defective intracellular transport of REST/NRSF mediated by the dynein–dynactin motor complex (60).

Whether NF-κB acts in the brain as a pro-survival or pro-apoptotic agent has been the topic of much debate. In recent years, however, it has become increasingly clear that tonic activation of NF-κB in neurons, driven by physiological levels of ongoing synaptic activity, is neuroprotective (17,18). In contrast, activation of NF-κB in glial cells, particularly in the context of acute brain injury, is neurotoxic (15). Activity-dependent BDNF expression is one component of the neuroprotective transcriptional response mediated by NF-κB in neurons (61,62) and is particularly relevant here because loss of BDNF expression has been proposed to play a critical role in the etiology of HD (7,8). In addition to loss of neuroprotection and activity-dependent BDNF expression, low levels of NF-κB activity in neurons could also lead to impairment of cognitive functions (63,64), a common feature of chronic neurodegenerative disorders such as HD.

In neurons, signals received at distal sites in axons and dendrites must be retrogradely transported to the nucleus to alter gene expression during neuronal development, synaptic plasticity and in response to neuronal injury. Recent studies

indicate that importins may mediate the transport of active-signaling cargoes, such as transcription factors and protein kinases, from dendritic spines and axon terminals back to the nucleus (65,66). For example, peripheral sensory neurons respond to axonal injury by assembling a signaling complex composed of an active-signaling cargo bound to a transport complex composed of importin-α, importin-β1 and the motor protein dynein. This signaling complex travels retrogradely along microtubular tracks from the site of injury in the periphery of the axon to the cell body where it elicits an adaptive transcriptional response (67,68).

We propose that Htt may serve a general role in neuronal transport similar to that of importin-β1, but in the context of synaptic transmission rather than axonal injury. Several recent findings support this idea. First, the primary and deduced secondary structures of Htt are similar to those of importin-β1. Like importin-β1, Htt is predominantly composed of repeated HEAT domains (14). This composition predicts a similar tertiary structure for the two proteins (69). Second, Htt is located in the PSD, closer to the synapse than importin-β1, which has a predominantly perinuclear localization and cannot be detected in the PSD fraction (51). Finally, we and others have found that importin-α2 (the usual binding partner of importin-β1) and its cargo NF-κB are both present in the PSD fraction (51) and interact with Htt. Therefore, we suggest that Htt may play a role similar to that of importin-β1 in the retrograde transport of NLS-containing cargoes from synapses toward the nucleus. The finding that a functional NLS is required for the retrograde transport of NF-κB in neurons and for the interaction between NF-κB and the dynein–dynactin motor complex (28) is consistent with this view. Thus, it would be worthwhile to determine whether Htt functions like importin-β1 with additional NLS-containing cargoes. Some of these, including NeuroD and REST/NSRF, are already known to interact with Htt (11–13).

A deeper understanding of the physiological function of wild-type Htt and its role in sustaining neuroprotective transcriptional homeostasis will inform the development of therapies for HD. In particular, the normal roles of Htt in neurons should be considered in the context of proposed cures based on silencing of *Htt* gene expression in the brains of HD patients.

MATERIALS AND METHODS

Animals

All procedures involving animals were carried out in accordance with the NIH Guide for the Care and Use of Laboratory Animals and were approved by the Institutional Animal Care and Use Committee (IACUC) of the California Institute of Technology. The HD 140Q knock-in mice are described in Menalled *et al*. (44) and were bred to generate homozygous mutants (HD) and wild-type littermate controls (WT). The Htt R1ag5 knock-out mice are described in Dragatsis *et al*. (4) and were bred to generate $Hdh^{flox}/-;Cre/+$ mutants (KO) and littermate controls lacking the *Cre* transgene (CTRL). Rats (Sprague–Dawley) were obtained from Harlan Laboratories.

Subcellular fractionation

S1 (post-nuclear supernatant), S2, P2 (crude synaptosomal pellet), SS (purified synaptosomal fraction), SUP ('One Triton' supernatant) and PSD ('One Triton' pellet) fractions were obtained from adult rat forebrains as described in Cho *et al*. (30) with minor modifications. S3 (cytosol) and P3 (microsomal pellet) fractions were obtained from the S2 fraction by ultracentrifugation (150 000*g*) for 1.5 h at 4°C. The CCV fraction was obtained from the P3 fraction as described in Velier *et al*. (35). Lipid rafts were obtained from the PSD fraction as described in Ma *et al*. (39). To rapidly obtain the PSD fraction from a single mouse forebrain, synaptosomes were purified by differential and Percoll density gradient centrifugation as described in Dunkley *et al*. (70), except that only three layers of Percoll (GE Healthcare Life Sciences) were used (5, 10 and 20%) and protease inhibitors (Complete EDTA-free, Roche) were added to the buffers. Purified synaptosomes were then washed and resuspended in the PSD buffer [40 mM Tris–HCl, pH 8.1, 1× protease inhibitor cocktail (Roche, Complete EDTA-free)], extracted by adding 0.5% Triton X-100 and stirring for 15 min at 4°C, and centrifuged (40 000*g*) for 40 min at 4°C to obtain the PSD ('One Triton' pellet) fraction.

Expression vectors

We are grateful to Johannes A. Schmid (Medical University of Vienna, Vienna, Austria) for the pEGFP–p65 plasmid, Roger Y. Tsien (University of California, San Diego, CA, USA) for the mCherry plasmid, George H. Patterson and Jennifer Lippincott-Schwartz (National Institutes of Health, Bethesda, MD, USA) for the PA-GFP plasmid. The p65 cDNA (from the pEGFP-p65 plasmid) was cloned in frame and fused at the C-terminus of the photoactivatable green fluorescent protein (paGFP, from the PA-GFP plasmid) cDNA into the phCMV1 vector backbone (Genlantis) to generate the pPA–GFP–p65 plasmid. The mCherry cDNA (from the mCherry plasmid) was cloned into the phCMV1 vector backbone (Genlantis) to generate the phCMV1–mCherry plasmid. DNA was purified using a plasmid maxi prep kit (QIAGEN, EndoFree Plasmid Maxi Kit).

Cell culture and transfection

Cerebral cortices were dissected from the brain of mice at embryonic day 15–16 and mechanically triturated in ice-cold Hank's balanced salt solution (GIBCO/Invitrogen, Cat. No. 14170) supplemented with 10 mM HEPES (pH 7.2–7.5) (GIBCO/Invitrogen) and 1 mM sodium pyruvate (GIBCO/Invitrogen). Dissociated neurons and glial cells were seeded on 24-well glass bottom plates (MatTek) freshly coated with poly-D/L-lysine (Sigma-Aldrich) at a density of ∼50 000 neurons/well and maintained in Neurobasal medium (GIBCO/Invitrogen) supplemented with 2% B-27 (GIBCO/Invitrogen) and 0.5 mM GlutaMAX-I (GIBCO/Invitrogen). Cultured neurons were transfected at 14 days *in vitro* using NeuroFECT (Genlantis) according to manufacturer's instructions, except that they were exposed to NeuroFECT/DNA complexes for only 1 h, washed and

maintained overnight in conditioned cell culture medium to prevent neurotoxicity. Human cervix carcinoma (HeLa) (ATCC, CCL-2) cells were cultured in DMEM GlutaMAX-I medium (GIBCO/Invitrogen, Cat. No. 10569) supplemented with 10% fetal bovine serum (HyClone), 0.1 mM non-essential amino acids (GIBCO/Invitrogen) and 100 U/ml penicillin + 100 μg/ml streptomycin (GIBCO/Invitrogen). To stimulate NF-κB activity, HeLa cells were incubated with recombinant human TNF-α (R&D Systems) at a concentration of 20 ng/ml for 30 min.

Antibodies and immunoblotting

The sample total protein concentration was determined using a bicinchoninic acid assay (Pierce) against bovine serum albumin standards according to manufacturer's instructions. Samples were briefly heated to near boiling in SDS–PAGE sample buffer and cleared of insoluble material by brief centrifugation. Equal amounts of total protein from each sample were resolved on 8% minigels by SDS–PAGE and transferred to Immobilon-FL membranes (Millipore) (71). The membranes were blocked overnight at 4°C in Odyssey Blocking Buffer (LI-COR) with continuous mixing and then incubated with primary and secondary antibodies according to manufacturer's instructions. Primary antibodies included mouse monoclonal anti-CaMKIIα (Affinity BioReagents, Cat. No. MA1-048, 1:2500 dilution), mouse monoclonal anti-PSD-95 (Affinity BioReagents, Cat. No. MA1-048, 1:2500 dilution), mouse monoclonal anti-Synaptophysin (Sigma-Aldrich, Cat. No. S5768, 1:2500 dilution), rabbit polyclonal anti-synGAP (Affinity BioReagents, Cat. No. PA1-046, 1:2500 dilution), rabbit polyclonal anti-PSD-95 (custom made, Frances, 1:5000 dilution), mouse monoclonal anti-Htt (Chemicon, Cat. No. MAB2166, 1:2500 dilution), mouse monoclonal anti-clathrin heavy chain (Transduction Laboratories, Cat. No. 610499, 1:2500 dilution), mouse monoclonal anti-Importin-α2 (Transduction Laboratories, Cat. No. 610485, 1:5000 dilution), mouse monoclonal anti-HAP1 (Transduction Laboratories, Cat. No. 611302, 1:250 dilution); rabbit polyclonal anti-NF-κB p65 (Santa Cruz Biotechnology, Cat. No. sc-372, 1:1000 dilution), rabbit polyclonal anti-NF-κB p50 (Santa Cruz Biotechnology, Cat. No. sc-114, 1:1000 dilution), rabbit polyclonal anti-I-κBα (Santa Cruz Biotechnology, Cat. No. sc-371, 1:500 dilution), mouse monoclonal anti-I-κBα (Santa Cruz Biotechnology, Cat. No. sc-1643, 1:500 dilution), rabbit polyclonal anti-phospho-I-κBα S32 (Cell Signaling Technology, Cat. No. 9241, 1:1,000 dilution), mouse monoclonal anti-phospho-I-κBα S32/36 (Cell Signaling Technology, Cat. No. 9246, 1:1000 dilution) and mouse monoclonal anti-Lamin A/C (Cell Signaling Technology, Cat. No. 4777, 1:1000 dilution). Secondary antibodies included Alexa Fluor 680 goat-anti-rabbit or mouse IgG (Molecular Probes, 1:10 000 dilution) and IRDye 800 goat-anti-rabbit or mouse IgG (Rockland Immunochemicals, 1:10 000 dilution). The All Blue Precision Plus Protein (Bio-Rad) prestained standard was used as molecular weight marker. For digital archiving and quantitative analysis, the membranes were scanned with an Odyssey dual-channel infrared scanner (LI-COR) using the Odyssey image analysis software (LI-COR).

Immunoprecipitation

Fifty microliters of protein G magnetic beads (Dynabeads Protein G, DYNAL/Invitrogen) were washed and coupled with 5 μg of antigen-specific or isotype control antibody according to manufacturer's instructions. When required, the antibody was cross-linked to the beads using disuccinimidyl suberate (Pierce) according to manufacturer's instructions. Two hundred fifty micrograms of PSD fraction were solubilized in 500 μl of DOC lysis buffer [50 mM Tris–HCl, pH 8.5, 1% sodium deoxycholate, 1× protease inhibitor cocktail (Roche, Complete)] by incubation for 30 min at 37°C and then diluted with an equal volume of ice-cold Triton X-100 dilution buffer [50 mM Tris–HCl, pH 8.5, 2% Triton X-100, 1× protease inhibitor cocktail (Roche, Complete)]. In total, 10^7 HeLa cells were lysed in 1 ml of ice-cold NP-40 lysis buffer [50 mM Tris–HCl, pH 7.5, 150 mM sodium chloride, 1% NP-40, 1× protease inhibitor cocktail (Sigma-Aldrich, Cat. No. P8340)] by incubation for 30 min on ice with occasional mixing. Insoluble material was removed by brief centrifugation. Five hundred microliters of solubilized PSD fraction or HeLa cell lysate were incubated with the beads for at least 3 h at 4°C with continuous mixing. The beads were then washed four times with 1 ml of ice-cold lysis buffer and once with 1 ml of ice-cold PBS using a magnetic separation rack (New England BioLabs). The proteins bound to the beads were eluted with 50 μl of SDS–PAGE sample buffer and processed for immunoblotting as described above.

To quantify the amount of precipitated protein, the integrated intensity of the fluorescent signal for p65 or importin-α2 that immunoprecipitated with Htt was measured with an Odyssey dual-channel infrared scanner and the Odyssey image analysis software (LI-COR). These signals were then normalized to the intensity of the Htt signal in the same immunoprecipitate and compared under different experimental conditions.

Enzyme-linked sorbent assay

To assess the interaction between Htt and PSD-95, we developed a fluorescent variant of the ELSA as follows. Human thioredoxin (TRX)-tagged Htt exon 1 fusion protein containing a stretch of 16 glutamines and TRX-tag control protein were expressed and purified as described in Bennett *et al*. (72). Full-length rat His-tagged PSD-95 fusion protein was expressed and purified as described in Korkin *et al*. (73). Purified TRX-tagged Htt exon 1 (10 μg/ml in PBS) was added to the wells of an Immulon-1B 96-well ELISA microplate (100 μl per well) in triplicates. An equimolar amount of TRX-tag protein was used as negative control. The plate was then incubated overnight at 4°C with gentle shaking to allow for adsorption of the ligand. After adsorption, the wells were washed three times with 200 μl of PBS and blocked overnight at 4°C with 200 μl of Odyssey Blocking Buffer (LI-COR). After blocking, the wells were washed three times with 200 μl of PBS and various amounts of purified PSD-95 were then added (100 μl per well, in Odyssey Blocking Buffer diluted with an equal volume of PBS) in triplicates and allowed to interact with the ligand for 3 h at room temperature. After binding, the wells were washed three times with 200 μl of PBS + 0.1% Tween (PBS-Tw), the

primary rabbit polyclonal antibody anti-PSD-95 (custom made, Frances, 1:1000 dilution) was added (100 μl per well, in Odyssey Blocking Buffer diluted with an equal volume of PBS-Tw) and the plate was incubated for 1 h at room temperature. After incubation with the primary antibody, the wells were washed three times with 200 μl of PBS-Tw, the secondary Alexa Fluor 680 goat-anti-rabbit IgG antibody (Molecular Probes, 1:2000 dilution) was added (100 μl per well, in Odyssey Blocking Buffer diluted with an equal volume of PBS-Tw) and the plate was incubated for 30 min at room temperature. After incubation with the secondary antibody, the wells were washed three times with 200 μl of PBS-Tw and once with 200 μl of PBS. The integrated intensity of the specific fluorescent signal was measured with an Odyssey dual-channel infrared scanner (LI-COR) using the Odyssey image analysis software (LI-COR) and interpreted as directly indicative of the amount of PSD-95 specifically bound to Htt exon 1. The K_d of the interaction between PSD-95 and Htt exon 1 was calculated by curve fitting using the Prism software (GraphPad).

NF-κB DNA-binding assay

Neuronal nuclei were purified by OptiPrep (Axis-Shield, 60% iodinaxol solution) and sucrose density gradient centrifugation as follows. One mouse forebrain was homogenized in 2.4 ml of ice-cold homogenization buffer [HB;20 mM Tricine–KOH, pH 7.8, 0.25 M sucrose, 25 mM potassium chloride, 5 mM magnesium chloride, 1× protease inhibitor cocktail (Roche, Complete EDTA-free)]. The homogenate was adjusted to 6 ml with HB and mixed with 4 ml of 50% iodinaxol solution. The mixture was then centrifuged (10 000*g*) for 30 min at 4°C in a swinging-bucket rotor. The nuclear pellet was resuspended in 2.4 ml of HB and centrifuged (1000*g*) for 10 min at 4°C. The nuclear pellet was enriched for neuronal nuclei and the nuclear proteins were extracted as described in Kaltschmidt *et al*. (20).

The DNA-binding activity of NF-κB in the nuclear extract was analyzed by DNA pull-down assay as follows. Five hundred micrograms of streptavidin magnetic beads (New England BioLabs) were washed with 1 ml of buffer A (20 mM Tris–HCl, pH 7.5, 0.5 M sodium chloride, 1 mM EDTA) using a magnetic separation rack (New England BioLabs). After washing, the beads were resuspended in 50 μl of buffer A supplemented with 250 pmol of biotinylated double-stranded DNA oligonucleotides (Integrated DNA Technologies) containing a wild-type κB site [5′-AGTTGAGGGGACTTTCCCAGGC-3′], and incubated for 10 min at room temperature to allow for binding of the biotinylated oligonucleotides to the streptavidin beads. An equal amount of biotinylated oligonucleotides containing a mutant κB site [5′-AGTTGAGGCGACTTTCCCAGGC-3′] was used as negative control. The DNA-coated beads were then washed three times with 1 ml of buffer A and incubated for 30 min at room temperature in 400 μl of buffer B [20 mM Tris–HCl, pH 7.5, 20 mM sodium chloride, 1 mM dithiothreitol] supplemented with 50 ng/μl poly(dI-dC) and 100 μl of nuclear extract (1 mg/ml total protein concentration). The beads were washed three times in 1 ml of buffer C [20 mM Tris–HCl, pH 7.5, 100 mM sodium chloride, 1 mM dithiothreitol, 5% glycerol] and the DNA-bound proteins were eluted with 50 μl of SDS–PAGE sample buffer and processed for immunoblotting as described above.

Live cell imaging and image analysis

Cultured neurons were made from single-sibling embryos and one littermate pair (mutant and control) was imaged per experiment ($n = 1$) under identical conditions. Neuronal cultures were pretreated for 12 h with 1 μM TTX to abolish action potentials and silence network activity. Just before image acquisition, the cultures were gently washed with HEPES-buffered tyrode solution [10 mM HEPES–NaOH, pH 7.4, 110 mM sodium chloride, 10 mM glucose, 5.4 mM potassium chloride, 1.8 mM calcium chloride, 0.8 mM magnesium chloride] prewarmed to 37°C and in the absence of TTX to induce synaptic activity. During image acquisition, the cultures were maintained in HEPES-buffered tyrode solution at 37°C using a heated incubation chamber fitted around the microscope. Time-lapse images (frame size, 200 × 200 pixels; pixel size, 0.1 × 0.1 μm; pixel time: ∼2 μs) of living, transiently transfected, cultured (15 days *in vitro*) cortical pyramidal neurons were acquired as series of single 5 μm-thick optical sections at a frame rate of 0.66 Hz, using an inverted laser-scanning confocal microscope (Zeiss, LSM 510 Meta NLO + Axiovert 200 M) equipped with a 63X/1.4NA oil immersion objective (Zeiss, Plan-Apochromat). paGFP–p65 and mCherry were excited using an Argon (488 nm line) and HeNe (543 nm line) laser, respectively. A Titanium:Sapphire near-IR tunable pulsed laser (Coherent, Chameleon) was used for two-photon photoactivation of paGFP–p65 at 750 nm. The green and red fluorescent emissions were collected separately through a band-pass (500–530 nm) and low-pass (560 nm) filter, respectively. Laser power was kept at a minimum to minimize photobleaching and photocytotoxicity. Images were acquired keeping the red and green fluorescence signals within the dynamic range of the instrument. Identical acquisition parameters and settings were used for all image acquisitions in a given experiment. Image acquisition was performed using the LSM 510 (Zeiss) software, and image analysis was performed using the ImageJ software (National Institutes of Health, http://rsb.info.nih.gov/ij). The half-life ($t_{\frac{1}{2}}$) of the green fluorescence intensity exponential decay within a region of interest was calculated by curve fitting using the Prism software (GraphPad). After live cell imaging, neurons were fixed with 4% formaldehyde in PBS for 5 min at room temperature and subjected to the same routine outlined above.

Statistical analysis

All quantitative data were expressed as means ± SEM. The Student's *t*-test (two-tailed, paired) was used for two group comparisons. A *P*-value of <0.05 significance cut off was used.

SUPPLEMENTARY MATERIAL

Supplementary Material is available at *HMG* online.

ACKNOWLEDGEMENTS

We are grateful to Pamela Bjorkman (Caltech, Pasadena, CA, USA) for the Htt exon 1 protein, Tinh Luong (Caltech) for the PSD-95 protein, Scott Zeitlin (University of Virginia, Charlottesville, VA, USA) for the Htt R1ag5 knock-out mice, Mike Levine (UCLA, Los Angeles, CA, USA) for the HD 140Q knock-in mice, Mollie Meffert (Johns Hopkins University, Baltimore, MD, USA) and members of the Kennedy laboratory for helpful discussions, and Leslie Schenker for technical assistance.

Conflict of Interest statement. None declared.

FUNDING

This work was supported by the Hereditary Disease Foundation (New York, NY, USA); the Huntington's Disease Society of America (New York, NY, USA); and the National Institutes of Health [NS028710].

REFERENCES

1. The Huntington's Disease Collaborative Research Group (1993) A novel gene containing a trinucleotide repeat that is expanded and unstable on Huntington's disease chromosomes. *Cell*, **72**, 971–983.
2. Bates, G., Harper, P. and Jones, L. (2002) *Huntington's Disease*, Oxford University Press, Oxford.
3. Leavitt, B.R., van Raamsdonk, J.M., Shehadeh, J., Fernandes, H., Murphy, Z., Graham, R.K., Wellington, C.L., Raymond, L.A. and Hayden, M.R. (2006) Wild-type huntingtin protects neurons from excitotoxicity. *J. Neurochem.*, **96**, 1121–1129.
4. Dragatsis, I., Levine, M.S. and Zeitlin, S. (2000) Inactivation of Hdh in the brain and testis results in progressive neurodegeneration and sterility in mice. *Nat. Genet.*, **26**, 300–306.
5. Zhang, Y., Li, M., Drozda, M., Chen, M., Ren, S., Mejia Sanchez, R.O., Leavitt, B.R., Cattaneo, E., Ferrante, R.J., Hayden, M.R. *et al.* (2003) Depletion of wild-type huntingtin in mouse models of neurologic diseases. *J. Neurochem.*, **87**, 101–106.
6. Leavitt, B.R., Guttman, J.A., Hodgson, J.G., Kimel, G.H., Singaraja, R., Vogl, A.W. and Hayden, M.R. (2001) Wild-type huntingtin reduces the cellular toxicity of mutant huntingtin *in vivo*. *Am. J. Hum. Genet.*, **68**, 313–324.
7. Zuccato, C., Ciammola, A., Rigamonti, D., Leavitt, B.R., Goffredo, D., Conti, L., MacDonald, M.E., Friedlander, R.M., Silani, V., Hayden, M.R. *et al.* (2001) Loss of huntingtin-mediated BDNF gene transcription in Huntington's disease. *Science*, **293**, 493–498.
8. Baquet, Z.C., Gorski, J.A. and Jones, K.R. (2004) Early striatal dendrite deficits followed by neuron loss with advanced age in the absence of anterograde cortical brain-derived neurotrophic factor. *J. Neurosci.*, **24**, 4250–4258.
9. Strand, A.D., Baquet, Z.C., Aragaki, A.K., Holmans, P., Yang, L., Cleren, C., Beal, M.F., Jones, L., Kooperberg, C., Olson, J.M. *et al.* (2007) Expression profiling of Huntington's disease models suggests that brain-derived neurotrophic factor depletion plays a major role in striatal degeneration. *J. Neurosci.*, **27**, 11758–11768.
10. Imarisio, S., Carmichael, J., Korolchuk, V., Chen, C.W., Saiki, S., Rose, C., Krishna, G., Davies, J.E., Ttofi, E., Underwood, B.R. *et al.* (2008) Huntington's disease: from pathology and genetics to potential therapies. *Biochem. J.*, **412**, 191–209.
11. Marcora, E., Gowan, K. and Lee, J.E. (2003) Stimulation of NeuroD activity by huntingtin and huntingtin-associated proteins HAP1 and MLK2. *Proc. Natl Acad. Sci. USA*, **100**, 9578–9583.
12. Zuccato, C., Tartari, M., Crotti, A., Goffredo, D., Valenza, M., Conti, L., Cataudella, T., Leavitt, B.R., Hayden, M.R., Timmusk, T. *et al.* (2003) Huntingtin interacts with REST/NRSF to modulate the transcription of NRSE-controlled neuronal genes. *Nat. Genet.*, **35**, 76–83.
13. Zuccato, C., Belyaev, N., Conforti, P., Ooi, L., Tartari, M., Papadimou, E., MacDonald, M., Fossale, E., Zeitlin, S., Buckley, N. *et al.* (2007) Widespread disruption of repressor element-1 silencing transcription factor/neuron-restrictive silencer factor occupancy at its target genes in Huntington's disease. *J. Neurosci.*, **27**, 6972–6983.
14. Takano, H. and Gusella, J.F. (2002) The predominantly HEAT-like motif structure of huntingtin and its association and coincident nuclear entry with dorsal, an NF-κB/Rel/dorsal family transcription factor. *BMC Neurosci.*, **3**, 15.
15. Mattson, M.P. and Meffert, M.K. (2006) Roles for NF-κB in nerve cell survival, plasticity, and disease. *Cell Death Differ.*, **13**, 852–860.
16. Marini, A.M., Jiang, X., Wu, X., Tian, F., Zhu, D., Okagaki, P. and Lipsky, R.H. (2004) Role of brain-derived neurotrophic factor and NF-κB in neuronal plasticity and survival: from genes to phenotype. *Restor. Neurol. Neurosci.*, **22**, 121–130.
17. Bhakar, A.L., Tannis, L.L., Zeindler, C., Russo, M.P., Jobin, C., Park, D.S., MacPherson, S. and Barker, P.A. (2002) Constitutive nuclear factor-κ B activity is required for central neuron survival. *J. Neurosci.*, **22**, 8466–8475.
18. Fridmacher, V., Kaltschmidt, B., Goudeau, B., Ndiaye, D., Rossi, F.M., Pfeiffer, J., Kaltschmidt, C., Israel, A. and Memet, S. (2003) Forebrain-specific neuronal inhibition of nuclear factor-κB activity leads to loss of neuroprotection. *J. Neurosci.*, **23**, 9403–9408.
19. Tian, F., Hu, X.Z., Wu, X., Jiang, H., Pan, H., Marini, A.M. and Lipsky, R.H. (2009) Dynamic chromatin remodeling events in hippocampal neurons are associated with NMDA receptor-mediated activation of Bdnf gene promoter 1. *J. Neurochem.*, **109**, 1375–1388.
20. Kaltschmidt, C., Kaltschmidt, B., Neumann, H., Wekerle, H. and Baeuerle, P.A. (1994) Constitutive NF-κB activity in neurons. *Mol. Cell. Biol.*, **14**, 3981–3992.
21. Meffert, M.K., Chang, J.M., Wiltgen, B.J., Fanselow, M.S. and Baltimore, D. (2003) NF-κB functions in synaptic signaling and behavior. *Nat. Neurosci.*, **6**, 1072–1078.
22. Kaltschmidt, C., Kaltschmidt, B. and Baeuerle, P.A. (1993) Brain synapses contain inducible forms of the transcription factor NF-κB. *Mech. Dev.*, **43**, 135–147.
23. Wellmann, H., Kaltschmidt, B. and Kaltschmidt, C. (2001) Retrograde transport of transcription factor NF-κB in living neurons. *J. Biol. Chem.*, **276**, 11821–11829.
24. Caviston, J.P., Ross, J.L., Antony, S.M., Tokito, M. and Holzbaur, E.L. (2007) Huntingtin facilitates dynein/dynactin-mediated vesicle transport. *Proc. Natl Acad. Sci. USA*, **104**, 10045–10050.
25. Gauthier, L.R., Charrin, B.C., Borrell-Pages, M., Dompierre, J.P., Rangone, H., Cordelieres, F.P., De Mey, J., MacDonald, M.E., Lessmann, V., Humbert, S. *et al.* (2004) Huntingtin controls neurotrophic support and survival of neurons by enhancing BDNF vesicular transport along microtubules. *Cell*, **118**, 127–138.
26. Trushina, E., Dyer, R.B., Badger, J.D. II, Ure, D., Eide, L., Tran, D.D., Vrieze, B.T., Legendre-Guillemin, V., McPherson, P.S., Mandavilli, B.S. *et al.* (2004) Mutant huntingtin impairs axonal trafficking in mammalian neurons *in vivo* and *in vitro*. *Mol. Cell. Biol.*, **24**, 8195–8209.
27. Colin, E., Zala, D., Liot, G., Rangone, H., Borrell-Pages, M., Li, X.J., Saudou, F. and Humbert, S. (2008) Huntingtin phosphorylation acts as a molecular switch for anterograde/retrograde transport in neurons. *EMBO J.*, **27**, 2124–2134.
28. Mikenberg, I., Widera, D., Kaus, A., Kaltschmidt, B. and Kaltschmidt, C. (2007) Transcription factor NF-κB is transported to the nucleus via cytoplasmic dynein/dynactin motor complex in hippocampal neurons. *PLoS ONE*, **2**, e589.
29. Sun, Y., Savanenin, A., Reddy, P.H. and Liu, Y.F. (2001) Polyglutamine-expanded huntingtin promotes sensitization of *N*-methyl-D-aspartate receptors via post-synaptic density 95. *J. Biol. Chem.*, **276**, 24713–24718.
30. Cho, K.O., Hunt, C.A. and Kennedy, M.B. (1992) The rat brain postsynaptic density fraction contains a homolog of the *Drosophila* discs-large tumor suppressor protein. *Neuron*, **9**, 929–942.
31. Kennedy, M.B. (2000) Signal-processing machines at the postsynaptic density. *Science*, **290**, 750–754.
32. Song, C., Zhang, Y., Parsons, C.G. and Liu, Y.F. (2003) Expression of polyglutamine-expanded huntingtin induces tyrosine phosphorylation of *N*-methyl-D-aspartate receptors. *J. Biol. Chem.*, **278**, 33364–33369.

33. Hunt, C.A., Schenker, L.J. and Kennedy, M.B. (1996) PSD-95 is associated with the postsynaptic density and not with the presynaptic membrane at forebrain synapses. *J. Neurosci.*, **16**, 1380–1388.
34. Kornau, H.C., Schenker, L.T., Kennedy, M.B. and Seeburg, P.H. (1995) Domain interaction between NMDA receptor subunits and the postsynaptic density protein PSD-95. *Science*, **269**, 1737–1740.
35. Velier, J., Kim, M., Schwarz, C., Kim, T.W., Sapp, E., Chase, K., Aronin, N. and DiFiglia, M. (1998) Wild-type and mutant huntingtins function in vesicle trafficking in the secretory and endocytic pathways. *Exp. Neurol.*, **152**, 34–40.
36. Li, X.J., Li, S.H., Sharp, A.H., Nucifora, F.C. Jr, Schilling, G., Lanahan, A., Worley, P., Snyder, S.H. and Ross, C.A. (1995) A huntingtin-associated protein enriched in brain with implications for pathology. *Nature*, **378**, 398–402.
37. Gutekunst, C.A., Li, S.H., Yi, H., Ferrante, R.J., Li, X.J. and Hersch, S.M. (1998) The cellular and subcellular localization of huntingtin-associated protein 1 (HAP1): comparison with huntingtin in rat and human. *J. Neurosci.*, **18**, 7674–7686.
38. Hering, H., Lin, C.C. and Sheng, M. (2003) Lipid rafts in the maintenance of synapses, dendritic spines, and surface AMPA receptor stability. *J. Neurosci.*, **23**, 3262–3271.
39. Ma, L., Huang, Y.Z., Pitcher, G.M., Valtschanoff, J.G., Ma, Y.H., Feng, L.Y., Lu, B., Xiong, W.C., Salter, M.W., Weinberg, R.J. *et al.* (2003) Ligand-dependent recruitment of the ErbB4 signaling complex into neuronal lipid rafts. *J. Neurosci.*, **23**, 3164–3175.
40. Blahos, J. II and Wenthold, R.J. (1996) Relationship between *N*-methyl-D-aspartate receptor NR1 splice variants and NR2 subunits. *J. Biol. Chem.*, **271**, 15669–15674.
41. Chen, H.J., Rojas-Soto, M., Oguni, A. and Kennedy, M.B. (1998) A synaptic Ras-GTPase activating protein (p135 SynGAP) inhibited by CaM kinase II. *Neuron*, **20**, 895–904.
42. Harkiolaki, M., Lewitzky, M., Gilbert, R.J., Jones, E.Y., Bourette, R.P., Mouchiroud, G., Sondermann, H., Moarefi, I. and Feller, S.M. (2003) Structural basis for SH3 domain-mediated high-affinity binding between Mona/Gads and SLP-76. *EMBO J.*, **22**, 2571–2582.
43. Suzuki, T., Mitake, S., Okumura-Noji, K., Yang, J.P., Fujii, T. and Okamoto, T. (1997) Presence of NF-κB-like and IκB-like immunoreactivities in postsynaptic densities. *Neuroreport*, **8**, 2931–2935.
44. Menalled, L.B., Sison, J.D., Dragatsis, I., Zeitlin, S. and Chesselet, M.F. (2003) Time course of early motor and neuropathological anomalies in a knock-in mouse model of Huntington's disease with 140 CAG repeats. *J. Comp. Neurol.*, **465**, 11–26.
45. Hickey, M.A., Kosmalska, A., Enayati, J., Cohen, R., Zeitlin, S., Levine, M.S. and Chesselet, M.F. (2008) Extensive early motor and non-motor behavioral deficits are followed by striatal neuronal loss in knock-in Huntington's disease mice. *Neuroscience*, **157**, 280–295.
46. Colomer, V., Engelender, S., Sharp, A.H., Duan, K., Cooper, J.K., Lanahan, A., Lyford, G., Worley, P. and Ross, C.A. (1997) Huntingtin-associated protein 1 (HAP1) binds to a Trio-like polypeptide, with a rac1 guanine nucleotide exchange factor domain. *Hum. Mol. Genet.*, **6**, 1519–1525.
47. Xie, Z., Srivastava, D.P., Photowala, H., Kai, L., Cahill, M.E., Woolfrey, K.M., Shum, C.Y., Surmeier, D.J. and Penzes, P. (2007) Kalirin-7 controls activity-dependent structural and functional plasticity of dendritic spines. *Neuron*, **56**, 640–656.
48. Hayden, M.S. and Ghosh, S. (2008) Shared principles in NF-κB signaling. *Cell*, **132**, 344–362.
49. Fagerlund, R., Kinnunen, L., Kohler, M., Julkunen, I. and Melen, K. (2005) NF-κB is transported into the nucleus by importin α3 and importin α4. *J. Biol. Chem.*, **280**, 15942–15951.
50. Mosammaparast, N. and Pemberton, L.F. (2004) Karyopherins: from nuclear-transport mediators to nuclear-function regulators. *Trends Cell Biol.*, **14**, 547–556.
51. Thompson, K.R., Otis, K.O., Chen, D.Y., Zhao, Y., O'Dell, T.J. and Martin, K.C. (2004) Synapse to nucleus signaling during long-term synaptic plasticity; a role for the classical active nuclear import pathway. *Neuron*, **44**, 997–1009.
52. Engelender, S., Sharp, A.H., Colomer, V., Tokito, M.K., Lanahan, A., Worley, P., Holzbaur, E.L. and Ross, C.A. (1997) Huntingtin-associated protein 1 (HAP1) interacts with the p150Glued subunit of dynactin. *Hum. Mol. Genet.*, **6**, 2205–2212.
53. Li, S.H., Gutekunst, C.A., Hersch, S.M. and Li, X.J. (1998) Interaction of huntingtin-associated protein with dynactin P150Glued. *J. Neurosci.*, **18**, 1261–1269.
54. Patterson, G.H. and Lippincott-Schwartz, J. (2002) A photoactivatable GFP for selective photolabeling of proteins and cells. *Science*, **297**, 1873–1877.
55. Gray, N.W., Weimer, R.M., Bureau, I. and Svoboda, K. (2006) Rapid redistribution of synaptic PSD-95 in the neocortex *in vivo*. *PLoS Biol.*, **4**, e370.
56. Graham, R.K., Pouladi, M.A., Joshi, P., Lu, G., Deng, Y., Wu, N.P., Figueroa, B.E., Metzler, M., Andre, V.M., Slow, E.J. *et al.* (2009) Differential susceptibility to excitotoxic stress in YAC128 mouse models of Huntington disease between initiation and progression of disease. *J. Neurosci.*, **29**, 2193–2204.
57. Joshi, P.R., Wu, N.P., Andre, V.M., Cummings, D.M., Cepeda, C., Joyce, J.A., Carroll, J.B., Leavitt, B.R., Hayden, M.R., Levine, M.S. *et al.* (2009) Age-dependent alterations of corticostriatal activity in the YAC128 mouse model of Huntington disease. *J. Neurosci.*, **29**, 2414–2427.
58. Wang, J., Wang, C.E., Orr, A., Tydlacka, S., Li, S.H. and Li, X.J. (2008) Impaired ubiquitin-proteasome system activity in the synapses of Huntington's disease mice. *J. Cell Biol.*, **180**, 1177–1189.
59. Simmons, D.A., Rex, C.S., Palmer, L., Pandyarajan, V., Fedulov, V., Gall, C.M. and Lynch, G. (2009) Up-regulating BDNF with an ampakine rescues synaptic plasticity and memory in Huntington's disease knockin mice. *Proc. Natl Acad. Sci. USA*, **106**, 4906–4911.
60. Shimojo, M. (2008) Huntingtin regulates RE1-silencing transcription factor/neuron-restrictive silencer factor (REST/NRSF) nuclear trafficking indirectly through a complex with REST/NRSF-interacting LIM domain protein (RILP) and dynactin p150 Glued. *J. Biol. Chem.*, **283**, 34880–34886.
61. Lipsky, R.H., Xu, K., Zhu, D., Kelly, C., Terhakopian, A., Novelli, A. and Marini, A.M. (2001) Nuclear factor κB is a critical determinant in *N*-methyl-D-aspartate receptor-mediated neuroprotection. *J. Neurochem.*, **78**, 254–264.
62. Marini, A.M., Rabin, S.J., Lipsky, R.H. and Mocchetti, I. (1998) Activity-dependent release of brain-derived neurotrophic factor underlies the neuroprotective effect of *N*-methyl-D-aspartate. *J. Biol. Chem.*, **273**, 29394–29399.
63. Meffert, M.K. and Baltimore, D. (2005) Physiological functions for brain NF-κB. *Trends Neurosci.*, **28**, 37–43.
64. Kaltschmidt, B., Widera, D. and Kaltschmidt, C. (2005) Signaling via NF-kappaB in the nervous system. *Biochim. Biophys. Acta*, **1745**, 287–299.
65. Otis, K.O., Thompson, K.R. and Martin, K.C. (2006) Importin-mediated nuclear transport in neurons. *Curr. Opin. Neurobiol.*, **16**, 329–335.
66. Jordan, B.A. and Kreutz, M.R. (2009) Nucleocytoplasmic protein shuttling: the direct route in synapse-to-nucleus signaling. *Trends Neurosci.*, **32**, 392–401.
67. Perlson, E., Hanz, S., Ben-Yaakov, K., Segal-Ruder, Y., Seger, R. and Fainzilber, M. (2005) Vimentin-dependent spatial translocation of an activated MAP kinase in injured nerve. *Neuron*, **45**, 715–726.
68. Hanz, S., Perlson, E., Willis, D., Zheng, J.Q., Massarwa, R., Huerta, J.J., Koltzenburg, M., Kohler, M., van-Minnen, J., Twiss, J.L. *et al.* (2003) Axoplasmic importins enable retrograde injury signaling in lesioned nerve. *Neuron*, **40**, 1095–1104.
69. Li, W., Serpell, L.C., Carter, W.J., Rubinsztein, D.C. and Huntington, J.A. (2006) Expression and characterization of full-length human huntingtin, an elongated HEAT repeat protein. *J. Biol. Chem.*, **281**, 15916–15922.
70. Dunkley, P.R., Jarvie, P.E. and Robinson, P.J. (2008) A rapid Percoll gradient procedure for preparation of synaptosomes. *Nat. Protoc.*, **3**, 1718–1728.
71. Towbin, H., Staehelin, T. and Gordon, J. (1979) Electrophoretic transfer of proteins from polyacrylamide gels to nitrocellulose sheets: procedure and some applications. *Proc. Natl Acad. Sci. USA*, **76**, 4350–4354.
72. Bennett, M.J., Huey-Tubman, K.E., Herr, A.B., West, A.P. Jr, Ross, S.A. and Bjorkman, P.J. (2002) Inaugural article: a linear lattice model for polyglutamine in CAG-expansion diseases. *Proc. Natl Acad. Sci. USA*, **99**, 11634–11639.
73. Korkin, D., Davis, F.P., Alber, F., Luong, T., Shen, M.Y., Lucic, V., Kennedy, M.B. and Sali, A. (2006) Structural modeling of protein interactions by analogy: application to PSD-95. *PLoS Comput. Biol.*, **2**, e153.